JAAS

PAPER

Cite this: *J. Anal. At. Spectrom.*, 2018, **33**, 2195

Antimony speciation analysis by hydride trapping on hybrid nanoparticles packed in a needle trap device with electro-thermal atomic absorption spectrometry determination†

Ariel Maratta, *[a] Brian Carrizo,[b] Vanesa L. Bazán,[c] Gastón Villafañe,[c] Luis Dante Martínez[a] and Pablo Pacheco *[a]

Received 19th September 2018
Accepted 29th October 2018

DOI: 10.1039/c8ja00311d

rsc.li/jaas

Oxidized multiwall carbon nanotubes (oxMWCNTs) were combined with TiO_2 nanoparticles to obtain hybrid nanoparticles (HNPs). A miniaturized flow injection (FI) system was introduced for antimony speciation and a headspace vial was used for hydride generation. HNPs were introduced into a needle trap device (NTD) as a sorbent for antimony hydride preconcentration in gas phase trapping. Antimony hydrides were adsorbed on HNPs. Electrothermal Atomic Absorption Spectrometry (ETAAS) was used for determination. The synergistic effect of HNPs improves Sb adsorption compared to oxMWCNTs reaching the quantitative preconcentration of the analyte in 1 minute. However, $NaBH_4$ concentration, HCl concentration and the elution volume were selected as variables for optimization. A Box–Behnken design indicated that the optimal response is achieved using 0.5% $NaBH_4$ (m v^{-1}), 1.5 mol L^{-1} HCl and 40 μL volume of elution. After optimization a retention efficiency of 99.8% was achieved with a preconcentration factor of 100. The limits of detection (LOD) and quantification (LOQ) were 0.4 and 1.2 ng L^{-1}. The relative standard deviation was 7.9% ($n = 10$). The time of analysis was 14 minutes. The developed technique was successfully applied to the analysis of river water samples.

1. Introduction

Antimony (Sb) is a metalloid present in the environment at low concentrations. However, it can be found in high concentrations in different environmental, biological and geological sectors due to mobilization from minerals and rocks, as well as anthropogenic activities such as mining, military training, smelting and the use of pharmaceutical products and pesticides.[1] The natural content of antimony in freshwater systems is generated mainly through rock erosion and soil leaching. Antimony concentrations in uncontaminated freshwater bodies generally range from a few ng L^{-1} to 1 μg L^{-1}. However, it can reach hundreds of μg L^{-1} in polluted rivers.[2,3] The World Health Organization (WHO) states that the maximum concentration of antimony in drinking water should be 10 μg L^{-1}.[4]

Antimony is found in two oxidation states in the environment and can also form numerous organic and inorganic species that have different toxic and physicochemical properties. The inorganic antimony compounds are more toxic than their organic counterparts, where the toxicity of Sb(III) is 10 times greater than that of Sb(V). In natural water, Sb predominates in inorganic forms. The species distribution depends on a number of factors including pH, redox and concurrent oxidants/reducers within a system.[1,5] Therefore, while Sb(V) is typically dominant it is difficult to simply deduce the antimony distribution under different environmental conditions. According to the low antimony concentrations and the necessity of identification of antimony species according to their different toxicity, hyphenated techniques are required to achieve species determination. They include sophisticated techniques like liquid chromatography coupled to inductively coupled plasma mass spectrometry (LC-ICP MS).[6,7]

Recently, simple preconcentration strategies for metals have been introduced, employing nanoparticles to increase adsorption and surface modification for selectivity. An interesting alternative is retention of hydride volatile species of metals which results in gas phase trapping techniques.[8,9] Nanoparticles are usually introduced for hydride trapping in minicolumns. Recently a novel solid phase extraction (SPE) configuration has been described, employing a needle instead of minicolumns.[10]

[a]*Instituto de Química de San Luis, INQUISAL, Centro Científico-Tecnológico de San Luis (CCT-San Luis), Consejo Nacional de Investigaciones Científicas—Universidad Nacional de San Luis, Chacabuco y Pedernera, Ciudad de San Luis 5700, Argentina. E-mail: ppacheco@unsl.edu.ar; arielmaratta@gmail.com*

[b]*Instituto de Ciencias Básicas, FFHA, Universidad Nacional de San Juan, Av. Libertador San Martin 1109—Oeste, 5400 San Juan, Argentina*

[c]*CONICET, Instituto de Investigaciones Mineras, Facultad de Ingeniería. UNSJ, Av. Libertador San Martín 1109(O), San Juan, 5400 Argentina*

† Electronic supplementary information (ESI) available. See DOI: 10.1039/c8ja00311d

The needle trap device (NTD) consists of a sorbent material, packaged inside a stainless steel needle. It is a robust and easy-handling device during sampling and desorption.[11–13] Since elution can be achieved with volumes in the order of microliters, the NTD can be coupled in line with sensitive techniques such as electrothermal atomic absorption spectrometry (ETAAS).

The key to achieve efficient isolation and preconcentration of the analyte in the NTD depends on sorbents with high sorption capacity at low quantities, according to the minimal size of needles in the NTD.[13] Multiwall carbon nanotubes (MWCNTs) have remarkable and outstanding characteristics to be used as sorbents in the NTD.[14] MWCNTs due to their large surface area can support adsorption materials to prepare new hybrid materials. Hybrid nanoparticles (HNPs) based on TiO_2 and CNTs have been used with different applications like electrical, catalytic, optical and detection.[15–17] Recently, hybrid materials have shown unique adsorption properties. The objective of preparation and design of hybrid materials is to take advantage of the best properties of two types of chemical compounds, organic and inorganic, with complementary properties in a single material.[18–20]

The potential of combining oxidized MWCNTs (oxMWCNTs) with TiO_2 nanoparticles to form HNPs and using them as a sorbent was studied. HNPs were introduced into an NTD for SPE of gaseous antimony hydrides. A flow injection (FI) system was design for hydride generation and speciation analysis. A headspace (HS) vial was used for gas generation and antimony was determined by electrothermal atomic absorption spectrometry (ETAAS). The study of the different variables affecting the system was carried out through a multivariate experimental design. Since antimony can be present in river water used for agricultural irrigation, the optimized technique was applied to antimony analysis in river water samples, to evaluate possible Sb entrance into the food chain.

2. Experimental

2.1. Reagents

Unless otherwise stated, the chemicals used were of analytical grade, and therefore no further purification was required. A 0.6% (w/v) sodium borohydride solution (Aldrich Chemical Co. 98%) was prepared in 0.5% (w/v) sodium hydroxide solution and was filtered through Whatman No. 42 filter paper to remove undissolved solids. This solution was prepared daily.

To prepare the Sb(III) standard stock solution at 1000 mg L^{-1}, 0.1334 g of antimony potassium-(C) tartrate salt (A.R., BDH) was dissolved in 1000 mL of a 3.0 mol L^{-1} HCl solution. For the 1000 mg L^{-1} Sb(V) standard stock solution, 1.05 mL of $SbCl_5$ (99.999%, Alfa) was diluted to 1000 mL in a volumetric flask with a 5 mol L^{-1} HCl solution.

Titanium dioxide (TiO_2) was obtained from Sigma-Aldrich Laboratories (St. Louis, USA). Thiourea (99% pure) was obtained from Sigma-Aldrich Laboratories (St. Louis, USA). Buffer solution (pH 8.0) was prepared with 50 mL of 0.1 mol L^{-1} KH_2PO_4 and 46.7 mL of 0.1 mol L^{-1} NaOH diluted to a final volume of 100 mL. Urea was acquired from Merck, Darmstadt, Germany.

MWCNTs were obtained from Sigma-Aldrich (St. Louis, USA). H_2SO_4, HNO_3, H_2O_2, and HCl used for the functionalization of MWCNTs as well as the digestion and treatment of samples were from Merck, Darmstadt, Germany.

Chemical modifiers for antimony atomization in ETAAS were prepared by dissolving the solid salt in deionized water (100 mL reaching a concentration of 10.000 mg L^{-1}). For the magnesium chemical modifier, 10.5495 g of $Mg(NO_3)_2 \cdot 6H_2O$ (Merck, Darmstadt, Germany) were weighed and diluted to 100 mL; for the palladium chemical modifier, 2.16 g of palladium nitrate (Merck, Darmstadt, Germany) were weighed and diluted to 100 mL.

2.2. Samples

River water samples were collected in San Juan province, Argentina. Upstream river water samples were obtained in Río Blanco, left side: 30°03′02.19″S, 69°10′10.96″W. Downstream river water samples were obtained in Río Jáchal, right side: 30°39′27.21″S, 68°32′54.36″W. Once collected, the samples were refrigerated to 4 °C avoiding microorganism activity and analyzed within 24 hours after sampling to avoid species interconversion.[21]

2.3. Apparatus

Gilson Minipuls 4 peristaltic pumps (Villiers, Le-Bell, France) and Tygon-type pump tubes (Ismatec, Cole-Parmer Instrument Company, Niles, IL, USA) were employed to propel the sample, eluent and reagents. Headspace vials (20 mL) and accessories were obtained from Perkin Elmer (Thornhill, Canada). These vials were used for antimony speciation, as well as for hydride generation. All unions were sealed to avoid gas losses. A magnetic stirrer was used in the HS vial during hydride generation.

The determination of Sb concentration was carried out on a Shimadzu Model AA-7000 atomic absorption spectrometer (Tokyo, Japan) equipped with a background correction system employing a continuum source, a GFA-EX7 electrothermal atomizer, and an ASC-7000 auto-sampler. L'vov graphite tubes (Shimadzu, Tokyo, Japan) were used in all experiments. An antimony hollow-cathode lamp (Hamamatsu, Photonics K. K., Japan) was employed as a radiation source at 6 mA and a wavelength of 217.5 nm with a spectral band pass of 1.0 nm. The graphite furnace temperature program is described in Table 1.

2.4. Synthesis of hybrid nanoparticles and needle trap device preparation

The synthesis of hybrid nanoparticles of oxMWNTCs and TiO_2 was carried out according to the methodology of Takenaka *et al.*[22], with modifications. Prior to the synthesis of HNPs, the MWCNTs were washed to eliminate metals, followed by oxidation according to the methodology described in previous studies.[10] The synthesis of HNPs consists in the use of oxMWCNTs as a support for TiO_2 nanoparticles. 100 mg of TiO_2 were weighed and dispersed in 50 mL of milli-Q water in a propylene tube. The oxMWCNTs in an equal quantity were dispersed by ultrasound in this solution at room temperature

Table 1 Graphite furnace temperature program

Graphite furnace temperature program for antimony determination				
Step	Temperature (°C)	Ramp time (s)	Hold time (s)	Ar flow (mL min^{-1})
Drying (I)	130	20	—	250
Drying (II)	1300	20	—	250
Atomization	1900	—	5	0
Cleaning	2500	—	3	250

for 40 min. Then, the mixture was transferred to a beaker and 33 mmol L^{-1} urea was added, where it was heated to 323 K with magnetic stirring for 120 min. After filtration, the obtained HNPs were dried at 333 K and calcined at 573 K for 60 min. HNPs were characterized according to the methodology described in the ESI.†

The needle trap device (NTD) was built using a stainless steel bevel needle with a length of 40 mm and an internal diameter of 0.5 mm. To avoid sorbent losses, the needle was preconditioned by placing glass wool in the needle bevel and applying heat to partially fuse the glass wool to generate a porous stopper. The needle was filled with 4 mg of HNPs by the wet packing method. Finally, glass wool was placed in the upper side of the needle.

2.5. Procedure

A simple headspace (HS) system was developed for antimony determination by micro-preconcentration of their volatile hydrides on HNPs (TiO_2-oxMWCNTs) contained in a needle trap device (NTD). As observed in Fig. 1, the system consists of a hermetically sealed 20 mL headspace vial, a valve that allows a preconcentration stage (C) through recirculation and an elution stage (E), a 4-channel pump and a magnetic agitator. Prior to each analysis, HNPs were activated by circulating a buffer solution (pH = 8).

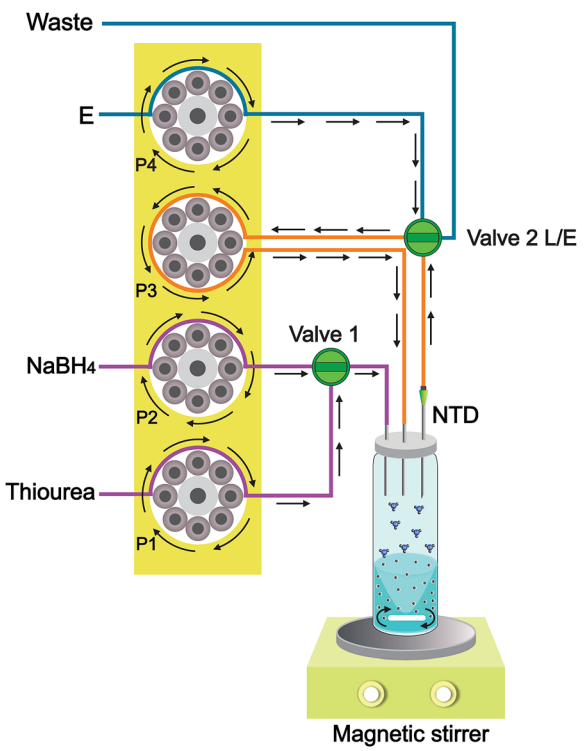

Fig. 1 Schematic diagram of the system used. Stage of HG/NTD. E, eluent; P, peristaltic pump; valve 2 L/E, loading and elution respectively; NTD, needle trap device loaded with HNPs.

In a first stage of sample preparation, 5 mL of river water sample, 0.5 mL of 1.5 mol L^{-1} HCl solution and a magnetic diver that allows constant agitation were placed in the HS vial. Then, the vial was sealed with a Teflon® partition.

In a second stage: hydride generation (HG) and preconcentration, the NTD is inserted through the septum. Two capillaries are also inserted that allow connecting the recirculation system and the addition of sodium borohydride and thiourea reagents. Once connected, the vial is placed on the magnetic stirrer at 20 rpm. Valve 2 is placed in the loading position (L). By means of pump P2 and valve 1 in the $NaBH_4$ position, 0.5 mL of 0.5% (m v^{-1}) $NaBH_4$ is added. During this step a gaseous antimony hydride is formed, being released from the liquid matrix. The antimony hydride is circulated with pump P3. The pump channel P4 is filled with the eluent to avoid gas losses. During this preconcentration approach only Sb(III) was separated. The procedure of antimony speciation was achieved by addition of 0.5 mL of 2 M thiourea solution (with 2 mol L^{-1} HCl) as a reducing reagent, through pump P1 and valve 1 in the thiourea position. The solution was stirred for 4 minutes. Total antimony was determined. Sb(V) is determined from the difference between total Sb and Sb(III).

Immediately after HG, the NTD is mounted on the robotic arm of an ETAAS autosampler for elution in a graphite furnace. The elution stage is achieved by propelling 40 μL of 5% HNO_3 (v/v) with pump P4 and valve 2 in the E position. The modifier (5 μL of Pd and Mg) was co-injected with the eluent.

3. Results and discussion

3.1. Characterization of HNPs

The modifications introduced to HNP synthesis led to a decrease in reagent consumption and synthesis time by direct introduction of TiO_2 instead of TiO_2 precursors. The hybrid nanoparticles that we describe in the present work were prepared by means of urea-mediated binding between oxMWCNTs and TiO_2. Urea acts as a binding molecule between the TiO_2 nanoparticles and the CNT surface, being eliminated during the calcination stage. In Fig. 2 the X-ray diffraction (XRD) pattern of the synthesized HNPs

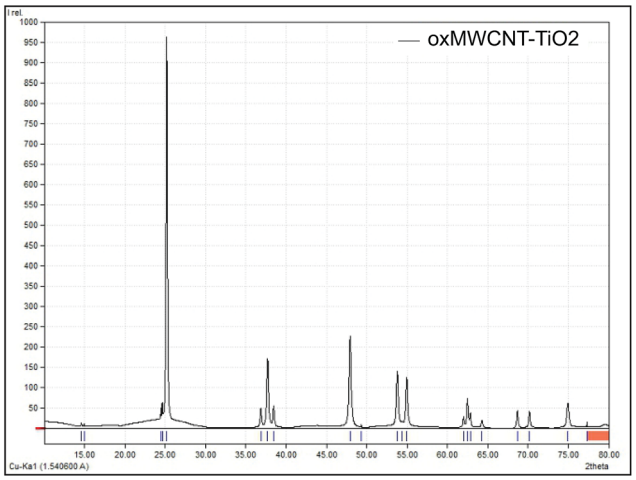

Fig. 2 XRD patterns of hybrid nanoparticles of oxMWCNTs-TiO_2.

is shown. This XRD pattern correspondent to other reported patterns in the bibliography for TiO_2–CNT NPs. Slight differences can be explained considering that the same components were used, but under different synthesis approaches. The peak present at $2\theta = 26^\circ$ is assigned to the reflection of the graphitic basal plane (0 0 2) of the CNTs. On the other hand, the characteristic diffraction peaks of TiO_2 are observed in an anatase phase at 25° and 48°.[23,24]

The fine morphology of the HNPs was evaluated by Scanning Electron Microscopy (SEM) (Fig. 3). As can be seen in Fig. 3A and B in a lower magnification image, the HNPs are a homogeneous material, where CNT agglomerations are not visible. This is repeated in Fig. 3C and D, with a greater zoom, where fibrous surfaces are perceived, exfoliated with a certain roughness. These results correspondent to other reported results in the literature.[25,26]

3.2. Hybrid nanoparticles *versus* oxidized multiwall carbon nanotubes

A comparison of the sorbent capacity between TiO_2-oxMWCNT hybrid nanoparticles and oxMWCNTs was made. In this study, two NTDs filled with 4 mg of each sorbent were prepared and the proposed methodology was implemented with a standard Sb solution of 40 ng L^{-1}. The Sb hydride circulation was evaluated in a range of 1–4 minutes, observing maximum retention at 4 minutes for both sorbents. However after 1 minute, HNPs retained 98.7% while oxMWCNTs retained 23.9% of antimony. The total preconcentration of the analyte is reached with HNPs in less than 1 minute, reducing the time of analysis to 3 minutes compared to oxMWCNTs. The improved sorption characteristics of HNPs can be explained considering several factors. The hybrid material has a larger surface area than oxMWCNTs increasing the number of active adsorption sites.[27–29] The combination of TiO_2 and the oxidized MWCNTs generates new active sites with an increased affinity for ionic species.[17,24] In addition, HNPTs do not form clusters, that could lead to back pressure problems, which are very common in SPE systems that use CNTs as sorbents.[20]

3.3. Solid phase extraction studies

Miniaturization is an important characteristic to consider when analytical methods are developed, in agreement with green chemistry principles.[30] In this study, a volume of 5 mL of sample was established for 20 mL vials, which allows the generation of a headspace avoiding excessive internal pressure. The volume of the reagents, thiourea, HCl and $NaBH_4$, was set to 0.5 mL. The contact time of the hydride with the sorbent was uncertain, since it depended on the flow generated by the internal pressure of the system as a function of the formation of the hydride,

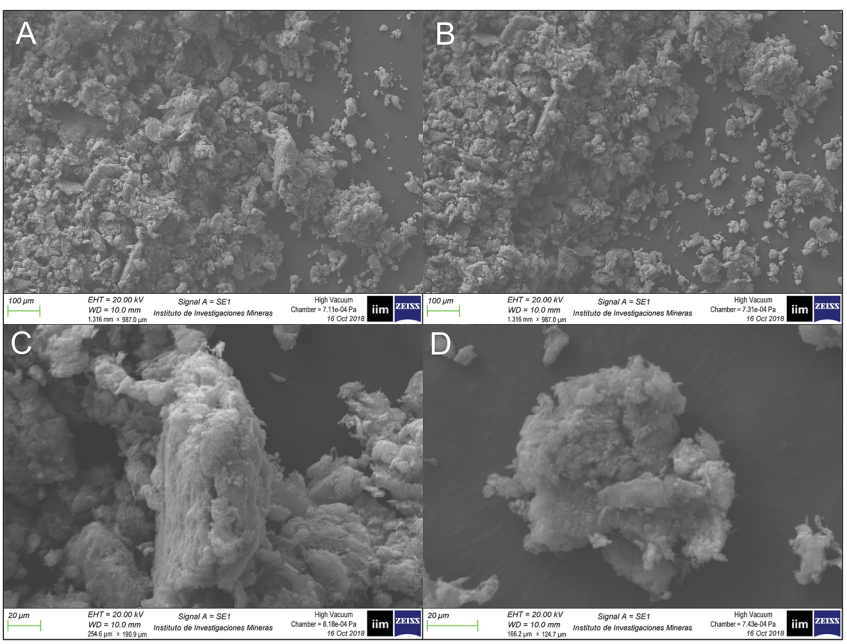

Fig. 3 Scanning electron micrographs of oxMWCNTs-TiO_2.

generating possible losses. This problem is overcome in the proposed FI system by the introduction of a controlled recirculation line at a flow rate of 1 mL min^{-1} in a totally closed system, which increases the interaction between the Sb hydride and the HNP, independently of the hydride generation rates.[8–10] Metal retention on carbon based solid sorbents has been deeply studied.[31] During antimony hydride sorption on HNP protonated species like stibonium ions (H_4Sb^+) can be formed.[32] This univalent cation can be electrostatically adsorbed on the HNP surface.

The elution stage, which consists in metal desorption from solid substrates, can be achieved through an exchange process between the metal ions adsorbed and H^+. Hydrochloric and nitric acids are the most commonly used chemicals to carry out elution.[33–35] In this study, nitric acid was selected for elution. Eluent concentration cannot exceed 5% (v/v) since higher concentrations shorten the life of the graphite tube.

Elution must be an instantaneous process with high recoveries.[36] However when recoveries are not quantitative, the elution flow rate can be decreased to enhance the contact time between the eluent and Sb-HNPs. In this sense, the elution flow rate was set at 0.25 mL min^{-1}. A low elution flow rate avoids spray generation in the furnace, affecting reproducibility during atomization. The selected elution flow rate also provides a uniform formation of the eluent drop on the platform of the graphite tube.

3.4. Multivariate optimization

In this research, after preliminary analysis and evaluation of some technical characteristics of the proposed system, parameters like sample volume, reagent volume and flow rate, gas recirculation rate and elution flow rate, were fixed at a single value. Only $NaBH_4$ concentration, HCl concentration and elution volume were selected as variables for optimization.

A multivariate strategy was adopted to investigate the influence of the selected variables and their interactions. The final optimization of the proposed methodology and the expected response according to the selected factors was carried out using the response surface method (RSM). A Box–Behnken design was exploited considering the most significant variables to determine the critical values for maximum absorption. A total of 15 experiments were performed with 3 central points to estimate the pure error. The factors that remained constant were set at: the flow rate of reagent addition and gas recirculation at 1 mL min^{-1}, 5 mL sample volume, 0.5 mL volume of HCl solution, 0.5 mL volume of $NaBH_4$, and the elution flow rate at 0.25 mL min^{-1}. For the speciation stage, 0.5 mL of a thiourea solution (2 mol L^{-1} thiourea; 2 mol L^{-1} HCl) was added.[37]

The selected factors as significant variables and their respective study ranges were $NaBH_4$ concentration (0.5–1.5%), HCl concentration (0.5–6 mol L^{-1}) and elution volume (20–50 μL). The response surfaces that highlight the regions of the optimal values are shown in Fig. 4(A, B, and C), with a graph of predicted values *versus* observed values (D), which indicate a good fit with a second order polynomial model. The analysis of variance indicated that the design was suitable for optimization, with an R-squared and adjusted R-squared of 0.984% and 0.995% respectively, with pure low errors (2.7×10^{-7}) at a confidence level of 95%. The response surfaces (Fig. 4) indicated that the optimal response is achieved using 0.5% $NaBH_4$ (m v^{-1}), 1.5 mol L^{-1} HCl and 40 μL volume of elution.

Fig. 4A graphically represents the response surface calculated as a function of the interaction of the HCl concentration and the elution volume, with a constant $NaBH_4$ concentration. It is observed that the optimal values are obtained by decreasing the acid concentration and increasing the elution volume. An increase in the concentration of acid can favor the generation of chloride species ($SbCl_3$ or $SbCl_5$), which interfere with the antimony hydride generation or antimony reduction in the speciation stage.[38,39] The elution efficiency increases with higher elution volumes, concluding that 40 μL are necessary to achieve a quantitative release of antimony hydrides from the NTD.

Fig. 4B and C show how the optimal $NaBH_4$ and HCl concentration is achieved by decreasing them. These observations are in good agreement with previous studies,[10] where an excess of these reagents generates undesired Sb species like chlorides and H_2, interfering with hydride generation and adsorption on HNPs respectively.

Subsequently, an experimental confirmation of the optimal conditions was made, where the response obtained was compared with that predicted with the model and no significant difference was observed with a confidence level of 95%.

3.5. Analytical characteristics of the proposed system

The time of analysis is an important characteristic of a developed methodology, directly related to reagent consumption, instrument running costs and analyst's work time. The proposed methodology decreases the time of analysis in 2 aspects. First, HNPs retained Sb hydrides in half the time compared to oxMWCNTs, maintaining quantitative retention. Second, a graphite furnace program without pyrolysis was applied and no differences in the Sb signal were observed.[40] According to these statements, the general time was calculated for the analysis of Sb(III) determination considering the stages of hydride generation and preconcentration, 0.5 min (0.5 mL of reagents at a flow rate of 1 mL min^{-1}); $NaBH_4$ addition and recirculation, 1 min (flow rate of 1 mL min^{-1}); elution, 0.16 min (40 μL at a flow rate of 0.25 mL min^{-1}); washing and conditioning (0.3 min); and heating cycle (0.9 min). For total Sb determination, a reduction step was previously carried out by adding the thiourea reagent (0.25 minutes at a flow rate of 2 mL min^{-1} and 4 minute of agitation). In both cases, a time of approximately 3 minutes is estimated to prepare the sample. The final time for antimony speciation per sample was 14 minutes, reaching a yield of ~4 samples per hour. HNPs were used for at least 100 cycles without loss of Sb retention efficiency.

Studies of analytical parameters were made following IUPAC recommendations.[41] Under optimal conditions, the precision of

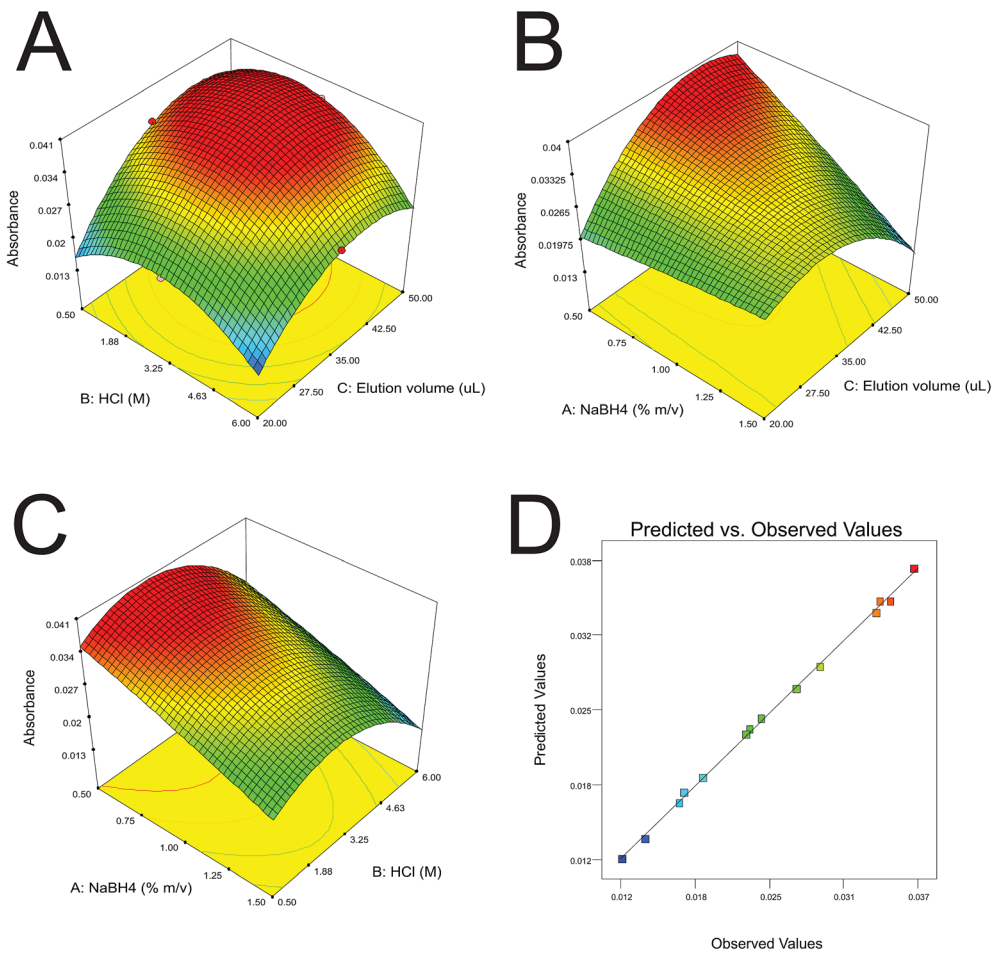

Fig. 4 Response Surfaces: (A) HCl (M) *x* elution volume (μL); (B) $NaBH_4$ (% m/v) *x* elution volume (μL); (C) $NaBH_4$ (% m/v) *x* HCl (M); (D) predicted *x* observed values obtained with Box–Behnken optimization.

the proposed methodology was evaluated and expressed as a relative standard deviation (RSD %) corresponding to 7.9% ($n = 10$). The RSD was determined by analyzing 10 replicates of a 70 ng L^{-1} Sb(III) solution. The system showed a linear calibration curve with a correlation coefficient of 0.9993 from levels close to the limit of quantification (LOQ) to at least 80 ng L^{-1}. The retention efficiency of the NTD at these concentration levels was 99.8%. Under these conditions, the limits of detection (LOD) and quantification (LOQ) were 0.4 and 1.2 ng L^{-1}, considering the measurement of ten blank solutions, for a sample volume of 5 mL. The preconcentration factor (PF) was calculated as the ratio of the final concentration of the analyte in the eluent phase and the concentration in the sample under optimal conditions. To calculate the PF of the analyte, preconcentration was performed under optimal conditions, and it corresponds to 100.

In Table 2, it is possible to observe a comparison of the analytical features of this method and others reported in the bibliography for Sb analysis with SPE. The proposed methodology represents many advantages like a lower LOQ and LD, with lower sample consumption and minimal use of reagents with an acceptable time of analysis.

3.6. Validation and application

There are no commercially available reference materials with a certified concentration of individual antimony species. However, QC Metal LL2 (Eurofins, Galten, Denmark) with a certified total antimony concentration was used for validation. Dilution was performed to encompass Sb concentration in the sample and the upper limit of the calibration range (80 ng L^{-1}). The CRM has a certified value for antimony of 49.1 ± 1.2 μg L^{-1} and the concentration of antimony obtained with the proposed system was 48.8 ± 3.1 μg L^{-1}. Speciation analysis was validated by standard addition. Tests were also performed on water samples, using solutions of Sb(III) and (V) species. Two samples were used in the experiments and the recoveries found varied from 98.4% to 102% for antimony(III) and from 98% to 104% for antimony(V). The obtained data are shown in Table 3. These results are conclusive to ensure that the proposed method can be used successfully for antimony determination in river water samples.

As observed in Table 3, downstream river water samples showed a higher antimony concentration, possible due to anthropogenic activities in the area and leaching. Antimony species distribution in downstream river water shows higher

Table 2 Comparison of methodologies for Sb analysis with solid phase extraction

Sample	Sample amount	Extraction	Sorbent	Analysis time	LD	LOQ	RSD (%)	Method	Reference
Water samples	50 mL	SPEME[a]	POIP[b]	>30 min	6 ng L^{-1}	20 ng L^{-1}	4.2	ETAAS	42
Natural water	40 mL	SPE	SWCNTs[c]	>30 min	2.1 ng L^{-1}	—	4.8	AFS[d]	43
Water samples	50 mL	SPE	CNTs	>20 min	50 ng L^{-1}	—	4	ETAAS	44
Environmental water	100 mL	MSPE[e]	C8-Fe_3O_4@SiO_2 NPs	>20 min	4 ng L^{-1}	—	4.6	ICP-MS	45
Water samples	10 mL	MSPE[e]	Fe_3O_4@Ag@MESNa NPs	>5 min	30 ng L^{-1}	—	5.6	ETAAS	46
Natural water	5 mL	NTD	HNPs (TiO_2-oxMWCNTs)	>13 min	0.4 ng L^{-1}	1.2 ng L^{-1}	7.9	ETAAS	This work

[a] SPEME: solid phase extraction-micro extraction. [b] POIP: polystyrene oleic acid imidazole polymer. [c] SWCNTs: single wall carbon nanotubes. [d] AFS: Atomic Fluorescence Spectroscopy. [e] MSPE: magnetic solid phase extraction.

Table 3 Recovery study – analysis of river water samples

		Base value (μg L^{-1})			Added value (μg L^{-1})	Found value (μg L^{-1})		Recovery%	
Sample	Aliquot	Sb(III)	Sb(V)	Sb total	Sb(III)/Sb(V)	Sb(III)	Sb(V)	Sb(III)	Sb(V)
Upstream water	1	0.36 ± 0.08	0.09 ± 0.08	0.45 ± 0.08	—	—	—	—	—
	2	0.36 ± 0.08	0.09 ± 0.08	0.45 ± 0.08	0.5	0.852 ± 0.08	0.61 ± 0.08	98.4[a]	104[a]
	3	0.36 ± 0.08	0.09 ± 0.08	0.45 ± 0.08	1	1.38 ± 0.08	1.07 ± 0.08	102[a]	98[a]
Downstream water	1	0.96 ± 0.08	3.84 ± 0.08	4.8 ± 0.08	—	—	—	—	—
	2	0.96 ± 0.08	3.84 ± 0.08	4.8 ± 0.08	0.5	1.454 ± 0.08	4,33 ± 0,08	98.8[a]	98[a]
	3	0.96 ± 0.08	3.84 ± 0.08	4.8 ± 0.08	1	1.965 ± 0.08	4.839 ± 0.08	100.5[a]	99.9[a]

[a] Sb 100 × (found-base)/(added). [b] Confidence intervals: $t_{(0.05,df)}S/(n)^{0.5}$. Informed values are average values of three replicate determinations ($n = 3$).

Sb(V) concentration compared to upstream water, where Sb(III) is elevated.

Interference can occur during hydride generation and hydride trapping on HNPs. No interference was observed during hydride generation in the Sb concentration working range. Since only hydrides reach the sorbent, other hydride forming elements and hydrogen could compete and interfere with Sb hydride trapping. Other hydride forming elements do not interfere with Sb hydride trapping at the concentrations they are present in the analyzed samples.

4. Conclusion

HNPs of TiO_2-oxMWCNTs adsorbed Sb hydrides on their surface. HNPs showed a quantitative adsorption performance compared to other methods reported in the bibliography for single nanoparticles. This performance can be explained considering some characteristics of HNPs, like the presence of higher and new active adsorption sites, and no cluster formation, that could lead to back pressure problems. In addition, a faster absorption on HNPs allowed a higher throughput sample.

HNPs were introduced into a NTD. This configuration allowed a miniaturized HG-SPE design. The design shows features like minimal reagent consumption, air tightness and semi-automation with flow injection. In this context a recirculation line increases Sb hydride adsorption on HNPs. A miniaturized design allowed setting minimal volumes and flow rates of reagents, leading to a simple and faster optimization with fewer variables. A FI design allowed Sb speciation through a pre-reduction step.

The proposed method achieves Sb determination in natural water at ultra-trace (ng L^{-1}) concentration levels, with minimal sample consumption. HNPs improve the analytical performance of the SPE method compared to other nanoparticles and sorbents reported in the literature.

Conflicts of interest

There are no conflicts to declare.

Acknowledgements

The authors wish to acknowledge the financial support received from the National Council of Scientific and Technical Research (CONICET), the National University of San Luis (UNSL), the National University of San Juan and the National Agency for Technical and Scientific Promotion (ANPCyT). The authors also thanks the Applied Geography Institute of San Juan (IGA).

References

1 I. Herath, M. Vithanage and J. Bundschuh, *Environ. Pollut.*, 2017, **223**, 545–559.
2 J. Li, B. Zheng, Y. He, Y. Zhou, X. Chen, S. Ruan, Y. Yang, C. Dai and L. Tang, *Ecotoxicol. Environ. Saf.*, 2018, **156**, 125–134.
3 H. Tian, D. Zhao, K. Cheng, L. Lu, M. He and J. Hao, *Environ. Sci. Technol.*, 2012, **46**, 3973–3980.

4 F. Edition, *WHO Chron.*, 2011, **38**, 104–108.
5 Y. Cai, Y. Mi and H. Zhang, *J. Hazard. Mater.*, 2016, **316**, 102–109.
6 M. Tighe, M. Edwards, G. Cluley, L. Lisle and S. Wilson, *J. Hydrol.*, 2018, **563**, 84–91.
7 N. R. Biata, L. Nyaba, J. Ramontja, N. Mketo and P. N. Nomngongo, *Food Chem.*, 2017, **237**, 904–911.
8 A. Maratta, L. D. Martinez and P. Pacheco, *Microchem. J.*, 2016, **127**, 199–205.
9 A. Maratta, M. Acosta, L. D. Martinez, P. H. Pacheco and R. A. Gil, *J. Anal. At. Spectrom.*, 2013, **28**, 916–922.
10 A. M. Martínez, S. Vázquez, R. Lara, L. D. Martínez and P. Pacheco, *Spectrochim. Acta, Part B*, 2018, **140**, 22–28.
11 J. Arndt, G. Ilgen and B. Planer-Friedrich, *J. Volcanol. Geotherm. Res.*, 2017, **331**, 16–25.
12 M. R. Azari, A. Barkhordari, R. Zendehdel and M. Heidari, *Microchem. J.*, 2017, **134**, 270–276.
13 K. Kędziora and W. Wasiak, *J. Chromatogr. A*, 2017, **1505**, 1–17.
14 H. L. Lord, W. Zhan and J. Pawliszyn, *Anal. Chim. Acta*, 2010, **677**, 3–18.
15 R. Yavari, N. Asadollahi and M. A. Mohsen, *Prog. Nucl. Energy*, 2017, **100**, 183–191.
16 Y. Zhang, B. Chen, S. Wu, M. He and B. Hu, *Talanta*, 2016, **154**, 474–480.
17 Y. Yan, J. Lu, C. Deng and X. Zhang, *Talanta*, 2013, **107**, 30–35.
18 Z. He and P. Alexandridis, *Adv. Colloid Interface Sci.*, 2017, **244**, 54–70.
19 M. Ahmadi, H. Elmongy, T. Madrakian and M. Abdel-Rehim, *Anal. Chim. Acta*, 2017, **958**, 1–21.
20 B. Fresco-Cala and S. Cárdenas, *Anal. Chim. Acta*, 2018, **1031**, 15–27.
21 T. Schulze, G. Streck and A. Paschke, in *Treatise on Water Science*, ed. P. Wilderer, Elsevier, Oxford, 2011, pp. 131–152, DOI: 10.1016/B978-0-444-53199-5.00054-3.
22 S. Takenaka, T. Arike, H. Matsune and M. Kishida, *Appl. Catal., B*, 2012, **125**, 358–366.
23 K. Thamaphat, P. Limsuwan and B. Ngotawornchai, *Kasetsart J.*, 2008, **42**, 357–361.
24 G. Fang, W. Gao, Q. Deng, K. Qian, H. Han and S. Wang, *Anal. Biochem.*, 2012, **423**, 210–217.
25 G. Papanicolaou and D. Portan, in *Structural Integrity and Durability of Advanced Composites*, Elsevier, 2015, pp. 735–761.
26 K. C. Silva, P. Corio and J. J. Santos, *Vib. Spectrosc.*, 2016, **86**, 103–108.
27 L. Wang, D. Hu, X. Kong, J. Liu, X. Li, K. Zhou, H. Zhao and C. Zhou, *Chem. Eng. J.*, 2018, **346**, 38–49.
28 D. Hu, X. Wan, X. Li, J. Liu and C. Zhou, *Int. J. Biol. Macromol.*, 2017, **105**, 1611–1621.
29 S. Ramesh, D. Vikraman, H.-S. Kim, H. S. Kim and J.-H. Kim, *J. Alloys Compd.*, 2018, **765**, 369–379.
30 M. Koel and M. Kaljurand, *Pure Appl. Chem.*, 2006, **78**, 1993–2002.
31 X. Liang, S. Liu, S. Wang, Y. Guo and S. Jiang, *J. Chromatogr. A*, 2014, **1357**, 53–67.
32 I.-S. Ke, M. Myahkostupov, F. N. Castellano and F. o. P. Gabbaï, *J. Am. Chem. Soc.*, 2012, **134**, 15309–15311.
33 A. Mehdinia, M. Ramezani and A. Jabbari, *Food Chem.*, 2017, **237**, 1112–1117.
34 M. A. El-Magied, A. G. S. Soliman, A. A. M. A. El-Hamid and E. Eldesouky, *J. Nucl. Mater.*, 2018, **509**, 295–304.
35 E. Yavuz, Ş. Tokalıoğlu and Ş. Patat, *Microchem. J.*, 2018, **142**, 85–93.
36 S. C. Moldoveanu and M. Kiser, *J. Chromatogr. A*, 2007, **1141**, 90–97.
37 P. H. Pacheco, R. A. Gil, L. D. Martinez, G. Polla and P. Smichowski, *Anal. Chim. Acta*, 2007, **603**, 1–7.
38 G. Ungureanu, S. Santos, R. Boaventura and C. Botelho, *J. Environ. Manage.*, 2015, **151**, 326–342.
39 W. A. Maher, F. Krikowa, S. D. Foster, M. J. Ellwood and W. W. Bennett, *J. Anal. At. Spectrom.*, 2018, **33**, 706–712.
40 D. J. Halls, *Analyst*, 1984, **109**, 1081–1084.
41 M. Thompson, S. L. Ellison and R. Wood, *Pure Appl. Chem.*, 2002, **74**, 835–855.
42 A. H. Panhwar, M. Tuzen, B. Hazer and T. G. Kazi, *Talanta*, 2018, **184**, 115–121.
43 H. Wu, X. Wang, B. Liu, Y. Liu, S. Li, J. Lu, J. Tian, W. Zhao and Z. Yang, *Spectrochim. Acta, Part B*, 2011, **66**, 74–80.
44 I. López-García, R. E. Rivas and M. Hernández-Córdoba, *Talanta*, 2011, **86**, 52–57.
45 Y. Liu, H. Li and J.-M. Lin, *Talanta*, 2009, **77**, 1037–1042.
46 I. López-García, S. Rengevicova, M. J. Muñoz-Sandoval and M. Hernández-Córdoba, *Talanta*, 2017, **162**, 309–315.